MOX-Report No. 22/2019

Optimized Schwarz methods for spherical interfaces with application to fluid-structure interaction

Gigante, G.; Sambataro, G.; Vergara, C.

Optimized Schwarz methods for spherical interfaces with application to fluid-structure interaction

G. Gigante[1], G. Sambataro[2], C. Vergara[3]

July 2, 2019

[1] Dipartimento di Ingegneria Gestionale, dell'Informazione e della Produzione
Università degli Studi di Bergamo, Italy
`giacomo.gigante@unibg.it`
[2] MOX– Modellistica e Calcolo Scientifico
Dipartimento di Matematica
Politecnico di Milano
`giulia.sambataro@mail.polimi.it`
[3] LABS, Dipartimento di Chimica, Materiali e Ingegneria Chimica "Giulio Natta"
Politecnico di Milano, Italy
`christian.vergara@polimi.it`

Abstract

In this work we consider the Optimized Schwarz method designed for computational domains that feature spherical or almost spherical interfaces. In the first part, we consider the diffusion-reaction problem. We provide a convergence analysis of the generalized Schwarz method, we discuss an optimization procedure for constant interface parameters leading to a Robin-Robin scheme, and we present some numerical results both in spherical and in ellipsoidal domains. In the second part of the work, we address the fluid-structure interaction problem. Again, we provide a convergence analysis and discuss optimal choices of constant interface parameters. Finally, we present 3D numerical results inspired by hemodynamic applications, to validate the proposed optimal choices in presence of large added mass effect. In particular, we consider numerical experiments both in an ideal spherical domain and in a realistic abdominal aortic aneurysm.

1 Introduction

The Optimized Schwarz Method (OSM) is an effective strategy to solve partial differential equations in a domain decomposition framework [13, 21, 23, 36]. In recent years, several improvements and applications of such a method have been provided by many authors. We mention, for example, the asynchronous update of the interface conditions [26], a posteriori error estimates [2], GPU-based solutions [25]. Also, analysis and applications for increasingly complex problems have been performed, for example for the Navier-Stokes equations [5], the gravitational potential problem [25], fluid-structure interaction [16,19], shallow-water equations [32], Maxwell's equations [9], Stokes-Darcy coupling [8].

Another field of study where a particular attention has been recently paid is the study of OSM for specific interface morphologies. This has been motivated by concrete applications where usually the interfaces among subproblems are not straight as in standard analyses of OSM. With this respect, we mention [24], where an analysis based on the Steklov-Poincaré operator has been obtained for general interfaces. Specific analyses and optimizations have been then performed for cylindrical [17–19,38] and circular interfaces [14,15,20].

In this work, we consider OSM for a new class of interfaces, namely the spherical ones. This is motivated by the application we have in mind, i.e. hemodynamics, where in some scenarios blood flows in domains which are of almost-spherical shape, as happens for example in abdominal and cerebral aneurysms and in the heart ventricles [33].

In the first part of the paper, we preliminarily focus on the diffusion-reaction problem (Sections 2, 3 and 4), whereas in the second one we study the fluid-structure interaction (FSI) problem, with the aim of addressing hemodynamic applications (Sections 5 and 6). In both cases, we provide a convergence analysis which allows us to obtain the corresponding reduction factors as a function of the interface symbols characterizing the interface conditions. Several numerical experiments are then shown. In particular, we consider two-dimensional axysymmetric simulations for the diffusion-reaction problem, both for spherical and ellipsoidal domains, and three-dimensional simulations for the FSI case, first in ideal spherical domains and finally in a realistic geometry of an abdominal aortic aneurysm. For all the numerical simulations, optimized interface constant symbols obtained by the abstract optimization procedure developed in [18] are used and compared with other non-optimal choices.

2 The diffusion-reaction problem

2.1 Problem setting

Given functions f, μ and γ, we consider the following problem in the sphere Ω with radius $R + H$:

Find u such that

$$
\begin{aligned}
-\mu \triangle u + \gamma u &= f && \text{in } \Omega, \\
u &= 0 && \text{on } \partial\Omega.
\end{aligned} \tag{1}
$$

Consider now an internal spherical interface Σ (whose center coincides with that of Ω) with radius R and, accordingly, split Ω into two non-overlapping subdomains, the sphere Ω_1 of radius R and the spherical shell Ω_2 with thickness H.

Then, problem (1) can be equivalently written in a multidomain formulation as follows:

Find u_1 and u_2 such that

$$
\begin{aligned}
-\mu \triangle u_1 + \gamma u_1 &= f && \text{in } \Omega_1, \\
u_1 &= u_2 && \text{on } \Sigma, && \text{(2a)} \\
\mu \frac{\partial u_1}{\partial r} &= \mu \frac{\partial u_2}{\partial r} && \text{on } \Sigma, && \text{(2b)} \\
-\mu \triangle u_2 + \gamma u_2 &= f && \text{in } \Omega_2, \\
u_2 &= 0 && \text{on } \partial\Omega,
\end{aligned}
$$

where r is the radial coordinate.

Introduce now the interface functions S_1 and S_2. Then, by linearly combining through such functions the interface conditions (2a)-(2b), we can introduce the following *Generalized Schwarz algorithm* for the solution of (1):

Let $u_2^{(0)}$ be given. Then, at each iteration $k > 0$, until convergence

1. Solve the subproblem in Ω_1:

$$
\begin{aligned}
-\mu \triangle u_1^{(k)} + \gamma u_1^{(k)} &= f && \text{in } \Omega_1, \\
S_1 u_1^{(k)} + \mu \frac{\partial u_1^{(k)}}{\partial r} &= S_1 u_2^{(k-1)} + \mu \frac{\partial u_2^{(k-1)}}{\partial r} && \text{on } \Sigma;
\end{aligned}
$$

2. Then, solve the subproblem in Ω_2:

$$
\begin{aligned}
-\mu \triangle u_2^{(k)} + \gamma u_2^{(k)} &= f && \text{in } \Omega_2, \\
S_2 u_2^{(k)} + \mu \frac{\partial u_2^{(k)}}{\partial r} &= S_2 u_1^{(k)} + \mu \frac{\partial u_1^{(k)}}{\partial r} && \text{on } \Sigma, \\
u_2^{(k)} &= 0 && \text{on } \partial\Omega.
\end{aligned}
$$

2.2 Convergence analysis

Referring to Figure 1, in view of the convergence analysis of iterations (3)-(4), we write the Laplacian operator in spherical coordinates as follows:

$$
\Delta_{sph} = \frac{1}{r^2} \frac{\partial}{\partial r} \left(r^2 \frac{\partial}{\partial r} \right) + \frac{1}{r^2 \sin^2 \varphi} \frac{\partial^2}{\partial \theta^2} + \frac{1}{r^2 \sin \varphi} \frac{\partial}{\partial \varphi} \left(\sin \varphi \frac{\partial}{\partial \varphi} \right).
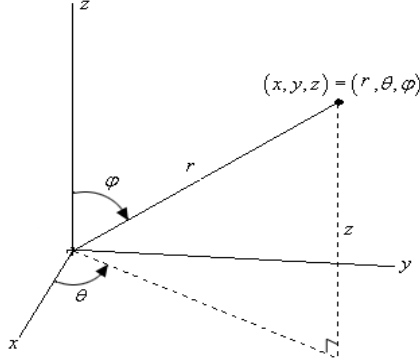$$

3

Figure 1: Spherical coordinates.

Now, set $\boldsymbol{x} = r\boldsymbol{x}'$, where $r = \|\boldsymbol{x}\|$ and $\boldsymbol{x}' = \boldsymbol{x}/\|\boldsymbol{x}\|$, and let

$$\left\{ P_{m,l}\left(\boldsymbol{x}'\right) \right\}_{m=0,l=1}^{+\infty,k_m}$$

be an orthonormal basis of spherical harmonics of the unit sphere S^2, where $k_m = (2m+1)$ is the dimension of the eigenspace associated with the eigenvalue $\lambda_m = m(m+1)$, $m = 0, \ldots, +\infty$, see, e.g., [12]. Then, for any function $v(\boldsymbol{x})$, let

$$\widehat{v}(r, m, l) = \int_{S^2} v\left(r\boldsymbol{x}'\right) \overline{P_{m,l}\left(\boldsymbol{x}'\right)} d\sigma\left(\boldsymbol{x}'\right) \tag{6}$$

be its Fourier transform with respect to $\boldsymbol{x}'$. Notice that the frequency variable m related to the spatial variable $\boldsymbol{x}'$ is discrete, since S^2 is a compact manifold.

In view of the convergence analysis, we introduce the modified Bessel functions of first and second kind I_ν and K_ν, see [22]. Moreover, set

$$\alpha = \sqrt{\frac{\gamma}{\mu}}, \qquad \chi = \frac{K_{m+\frac{1}{2}}\left((R+H)\alpha\right)}{I_{m+\frac{1}{2}}\left((R+H)\alpha\right)}. \tag{7}$$

As usual, we set $f = 0$ in order to analyze convergence towards the null solution.

We have the following result.

Proposition 1. *The convergence factor of iterations (3)-(4) is given by*

$$\rho(m) = \left| \frac{\sigma_1(m) - A(m)}{\sigma_2(m) - A(m)} \cdot \frac{\sigma_2(m) - B(m)}{\sigma_1(m) - B(m)} \right|, \tag{8}$$

where

$$A(m) = -\mu \frac{2\alpha R K'_{m+\frac{1}{2}}(\alpha R) - K_{m+\frac{1}{2}}(\alpha R) - 2\alpha R \chi I'_{m+\frac{1}{2}}(\alpha R) + \chi I_{m+\frac{1}{2}}(\alpha R)}{2R\left(K_{m+\frac{1}{2}}(\alpha R) - \chi I_{m+\frac{1}{2}}(\alpha R)\right)} \tag{9}$$

$$B(m) = -\mu \frac{2\alpha R I'_{m+\frac{1}{2}}(\alpha R) - I_{m+\frac{1}{2}}(\alpha R)}{2R I_{m+\frac{1}{2}}(\alpha R)}, \tag{10}$$

4

and σ_i are the Fourier symbols related to the interface operators S_i, $i = 1, 2$.

Proof. Following [18], by applying the Fourier transform (6) to problems (3) and (4), and by using (5), we obtain the following ordinary differential equations in the variable r:

$$r^2 \frac{\partial^2 \widehat{u}_i^{(k)}}{\partial r^2} + 2r \frac{\partial \widehat{u}_i^{(k)}}{\partial r} - \left(m(m+1) + \frac{\gamma}{\mu} r^2 \right) \widehat{u}_i^{(k)} = 0, \quad i = 1, 2. \qquad (11)$$

Through the change of variables $\widehat{u}_i^{(k)}(r) = v_i(\alpha r)/\sqrt{r}$, equations (11) become

$$v_i''(t) + \frac{1}{t} v_i'(t) - \left(1 + \frac{(m + \frac{1}{2})^2}{t^2} \right) v_i(t) = 0, \quad i = 1, 2.$$

These are modified Bessel equations and their solutions are given by the modified Bessel functions of first and second kind introduced above:

$$v_i(t) = X_{i,1} I_{m+\frac{1}{2}}(t) + X_{i,2} K_{m+\frac{1}{2}}(t), \quad i = 1, 2,$$

for suitable functions of the frequency $X_{i,j}$, $i, j = 1, 2$.

Thus, the Fourier transform of i-th solution at iteration $k > 0$ in the Generalized Schwarz algorithm (3)-(4) assumes the following form:

$$\widehat{u}_i^{(k)}(r, m, l) = X_{i,1}^{(k)}(m, l) \frac{I_{m+\frac{1}{2}}(\alpha r)}{\sqrt{r}} + X_{i,2}^{(k)}(m, l) \frac{K_{m+\frac{1}{2}}(\alpha r)}{\sqrt{r}}.$$

Since we assume that the solution u_1 is bounded for $r = 0$, we have

$$\widehat{u_1}^{(k)}(r, m, l) = X_1^{(k)}(m, l) \frac{I_{m+\frac{1}{2}}(\alpha r)}{\sqrt{r}}. \qquad (12)$$

Instead, due to the homogeneus Dirichlet condition at $\partial \Omega$

$$\widehat{u_2}^{(k)}(R+H, m, l) = X_{2,1}^{(k)}(m, l) \frac{I_{m+\frac{1}{2}}((R+H)\alpha)}{\sqrt{R+H}} + X_{2,2}^{(k)}(m, l) \frac{K_{m+\frac{1}{2}}((R+H)\alpha)}{\sqrt{R+H}} = 0,$$

we have

$$X_{2,1}^{(k)} = -\frac{K_{m+\frac{1}{2}}((R+H)\alpha)}{I_{m+\frac{1}{2}}((R+H)\alpha)} X_{2,2}^{(k)}.$$

Thus, we have

$$\widehat{u_2}^{(k)}(r, m, l) = \frac{X_2^{(k)}(m, l)}{\sqrt{r}} \left(K_{m+\frac{1}{2}}(\alpha r) - \chi I_{m+\frac{1}{2}}(\alpha r) \right), \qquad (13)$$

with χ given by (23).

Inserting the solutions (12)-(13) in the interface conditions of iterations (3)-(4) and proceeding as usual (see, e.g., [18]), it is now easy to show that the reduction factor related to (3)-(4) is given by (8)-(9)-(10).

$\square$

3 Optimization procedure and choice of the frequencies

In view of the numerical experiments, an optimization procedure is mandatory in order to select reliable values (e.g. among the constants) for the interface parameters σ_1 and σ_2. Specific optimization procedures could be in principle developed for the problem at hand. These would lead to optimal values of the interface parameters that should make the reduction factor small in comparison to other values for a wide range of frequencies m.

Here, instead, we consider the abstract optimization procedure developed in [18], which provides a range of "optimal" constant values for the interface parameters, thus leading to an optimized Robin-Robin scheme. With respect to specific procedures, this one is not able to determine the best choice for the interface parameters, rather only a range of good ones. On the other side, its great advantage is that it is completely general, thus ready to be applied to reduction factors related to a wide class of problems [19, 20].

For the sake of completeness, we review in what follows the abstract optimization procedure reported in [18]. For clarity purposes, we report it directly for the case we have in mind, where only the discrete frequency m is involved.

Assume that the reduction factor has precisely the form of (8) with A and B general functions of m. Assume also that $A(m)$ and $B(m)$ are bounded on some set K, with $B < A$ for all $m \in K$, and set

$$\overline{B} = \max_{m \in K} B(m), \qquad\qquad \overline{A} = \min_{m \in K} A(m),$$

$$\overline{M} = \frac{1}{2}(\overline{A} + \overline{B}), \qquad\qquad M(m) = \frac{1}{2}(A(m) + B(m)),$$

$$D(m) = \frac{1}{2}(A(m) - B(m)), \qquad\qquad \overline{Q} = \max_{m \in K} Q(m),$$

$$N = \frac{\min_{m \in K} D(m)}{\max_{m \in K} D(m)}, \qquad\qquad Q(m) = \frac{|M(m) - \overline{M}|}{D(m)}.$$

The procedure searches optimal values on a specific straight line in the plane σ_1, σ_2, namely

$$\begin{cases} \sigma_1 = p, \\ \sigma_2 = 2\overline{M} - p. \end{cases}$$

In particular, it is proven that, setting

$$\rho_0 = \max \left\{ \left(\frac{1 - \sqrt{N}}{1 + \sqrt{N}} \right)^2 ; \left(\frac{1 - \sqrt{1 - \overline{Q}^2}}{\overline{Q}} \right)^2 \right\},$$

for all $m \in K$, we have

$$\widehat{\rho}(p,m) = \left| \frac{p - A(m)}{-p + 2\overline{M} - A(m)} \frac{-p + 2\overline{M} - B(m)}{p - B(m)} \right| \leq \rho_0 \iff p \in [p_-, p_+],$$

with

$$p_- = \overline{M} + \sup_{m \in K} \left\{ \frac{1 + \rho_0}{1 - \rho_0} D(m) - \sqrt{\left(\overline{M} - M(m)\right)^2 + \frac{4\rho_0}{(1 - \rho_0)^2} (D(m))^2} \right\},$$

$$p_+ = \overline{M} + \inf_{m \in K} \left\{ \frac{1 + \rho_0}{1 - \rho_0} D(m) + \sqrt{\left(\overline{M} - M(m)\right)^2 + \frac{4\rho_0}{(1 - \rho_0)^2} (D(m))^2} \right\}.$$

The strong point of this result is that the range $[p_-, p_+]$ guarantees that the reduction factor is less than ρ_0 for any $m \in K$.

A crucial point from the practical point of view in the application of the previous result is played by the choice of the set of frequencies K. Indeed, different sets lead to different ranges $[p_-, p_+]$. In general, the set K is of the type $[m_{min}, m_{max}]$. We discuss in what follows three possible choices of the extreme points of such a range [20].

1. $\mathbf{m_{min} = 0, m_{max} = N - 1}$. The first choice consists in considering all the admissible frequencies which avoid the aliasing phenomenon for a given computational mesh. In this case $m_{min} = 0$, whereas we have $m_{max} = N-1$, where N is such that simple algebraic considerations ensure that aliasing appears as soon as one replaces $N - 1$ with any bigger number. In particular, by calling $Rx_1, \ldots, Rx_n$ the interface mesh nodes and expanding a function with respect to the eigenfunctions of the unit sphere $P_{m,l}$ introduced above, then, for a given function g, the linear system

$$\begin{cases} g(Rx_1) = \sum_{m=0}^{N-1} \sum_{l=1}^{2m+1} a_{m,l} P_{m,l}(x_1) \\ \ldots \\ \ldots \\ g(Rx_n) = \sum_{m=0}^{N-1} \sum_{l=1}^{2m+1} a_{m,l} P_{m,l}(x_n) \end{cases}$$

does not admit a unique solution if the number of unknowns $a_{m,l}$ (which is $\sum_{m=0}^{N-1} 2m + 1 = N^2$) is greater than the number of equations, i.e. the number of interface points n. Thus, we have that the number of admissible frequencies N is related to the number of interface nodes n by the relation $N = \sqrt{n}$;

2. $\mathbf{m_{min} = M_{min}, m_{max} = M_{max}}$. The second choice is based on observing that among the admissible frequencies $[0, N - 1]$ one expects that only a subset of frequencies $[M_{min}, M_{max}]$ could play a major role in determining the reduction factor. This choice could be motivated, for example, by the particular shape of the computational domain or by the problem at hand (pure diffusion, presence of advection, ...). The hope here is that focusing on a smaller effective range of frequencies, the optimization procedure could provide a better range $[p_-, p_+]$ in terms of convergence;

3. $\mathbf{m_{min}} = \mathbf{m_1}, \mathbf{m_{max}} = \mathbf{m_2}$. The last choice is provided by the minimum and maximum frequencies m_1 and m_2 appearing in the initial guess of the algorithm. The idea is that frequencies outside this range should not give a significant contribution to determining the reduction factor. This could again provide a better range $[p_-, p_+]$.

4 Numerical results for the diffusion-reaction problem

We present here some numerical results for the diffusion-reaction problem. These were obtained by considering 2D axi-symmetric simulations. In the first test (test-I) we consider a spherical computational domain, whereas in the second one (test-II) we consider an ellipsoidal domain.

In all the cases, cubic $P3$ Lagrangian Finite Elements and the open library Freefem++ (`www.freefem.otg`) have been used. Moreover, we set $\mu = \gamma = 1.0$, $f = 0.0$, and the mesh is such that $N = 31$. The initial guess is $u_2^{(0)} = \sum_{m=0}^{10} P_m(x/r)$, so that $m_1 = 0$ and $m_2 = 10$. Here, P_m are the Legendre polynomials and $P_m(x/r)$ is the only axi-symmetric spherical harmonic corresponding to the frequency variable m. The minimum frequency m_{min} used in the optimization procedure is always set equal to 0.

The stopping criteron is given by [3]

$$\int_\Sigma \sigma_1 \left| u_1^{(k)} - u_2^{(k)} \right| + \left| \mu \frac{\partial u_1^{(k)}}{\partial r} - \mu \frac{\partial u_2^{(k)}}{\partial r} \right| < \varepsilon,$$

with $\varepsilon = 10^{-7}$.

4.1 Results in a spherical domain

In this test, Ω is given by the rotation around the $x-$axis of half of a circle of radius $R_{tot} = 1.5$, see Figure 2. The interface Σ is obtained by rotating half of
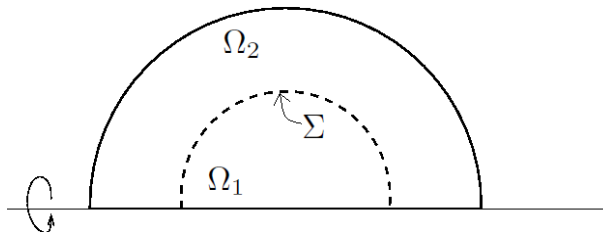

Figure 2: Computational domain for the axi-symmetric simulations.

the circumference of radius $R = 1.0$ around the $x-$axis. Thus, the thickness of the spherical shell Ω_2 is $H = 0.5$.

In what follows we report the convergence properties of numerical simulations obtained for different choices of m_{max}. For each case, the optimal range $[p_-, p_+]$ is evaluated.

1. $\boldsymbol{m_{max} = m_2 = 10}$. We suppose that the dominant frequencies are those appearing in the initial guess. By applying the optimization procedure, we obtain:

$$[p_-, p_+] = [5.669, 5.708], \quad \overline{M} = 1.425, \quad \rho_0 = 0.179.$$

2. $\boldsymbol{m_{max} = M_{max} = 20}$. We assume that other relevant frequencies than the initial ones appear during the iterations. By applying the optimization procedure, we obtain:

$$[p_-, p_+] = [7.386, 7.399], \quad \overline{M} = 1.425, \quad \rho_0 = 0.301.$$

3. $\boldsymbol{m_{max} = N - 1 = 30}$. We assume that all the admissible frequencies are relevent in determining the reduction factor. By applying the optimization procedure, we obtain:

$$[p_-, p_+] = [8.702, 8.710], \quad \overline{M} = 1.425, \quad \rho_0 = 0.378.$$

Notice that in all the three cases, the value of $\overline{M}$ is the same, thus the research of the optimal value is obtained by moving along the same straight line $s : \sigma_2 = -\sigma_1 + 2.85$.

In Table 1, we report the convergence results for different values of p that guarantee to be on this line. In particular, we consider the three optimal values σ_i^{optj}, $j = 1, 2, 3$, obtained a priori minimizing, for each of the three estimated ranges, the reduction factor for the values of σ_1 and σ_2 belonging to s. We also consider other values outside such ranges, still moving along the line s.

σ_1	$\sigma_2 = 2\overline{M} - \sigma_1$	# iter
$\sigma_1 = 2.00$	$\sigma_2 = 0.85$	54
$\sigma_1 = 4.00$	$\sigma_2 = -1.15$	17
$\sigma_1 = \sigma_1^{opt1} = 5.69$	$\sigma_2 = -2.84$	12
$\sigma_1 = \sigma_1^{opt2} = 7.39$	$\sigma_2 = -4.54$	14
$\sigma_1 = \sigma_1^{opt3} = 8.71$	$\sigma_2 = -5.86$	17
$\sigma_1 = 10.00$	$\sigma_2 = -7.15$	19
$\sigma_1 = 12.00$	$\sigma_2 = -9.15$	23
$\sigma_1 = +\infty$	$\sigma_2 = 0$	131

Table 1: Convergence properties for different values of the interface parameters. Test I.

From these results we observe that the optimal value is $p = 5.69$. This value perfectly falls down in the first of the three ranges given by the optimization procedure ($[5.669, 5.708]$), whose extreme points, due to its smallness, in fact provide

9

directly an excellent approximation of the optimal value. This is consistent with the value of ρ_0 which is the smallest one among the three estimates. This is probably due to the fact that in this case the smallest frequencies are the most relevant ones, since the initial guess does not contain frequencies greater than 10. Thus, in the optimization procedure it is enough to consider as maximum frequency m_{max}, i.e. the greatest one appearing in the initial condition.

We notice also the great improvement of the generalized Schwarz (Robin-Robin) algorithm with respect to the Dirichlet-Neumann one ($\sigma_1 = +\infty$, $\sigma_2 = 0$) with an Aitken acceleration procedure [7, 34].

4.2   Results in an ellipsoidal domain

In the next numerical experiment, we consider a computational domain which is not a sphere. Indeed, our hope is that our spherical analysis and optimization procedure provide effective values of the interface parameters also for non-spherical interfaces, provided that the shape of the domain and of the interface is almost spherical. In this case, we do not obtain the optimal values for such a configuration, but however we expect to obtain excellent approximations.

To this aim, we consider an ellipsoidal domain with semi-axis equal to $a+H$, $b+H$ and $b+H$ for the x, y and z direction, respectively, obtained by a rotation around the $x-$axis of the ellipse with semi-axis equal to $a + H$ ($x-$direction) and $b + H$ ($y-$direction). The interface Σ is obtained by rotating around the $x-$axis half of the ellipse with semi-axis of length a and b.

For the choice of the radius of the sphere to be used in the analysis and optimization procedure for the computation of A and B in (9)-(10), we study the numerical performance of four different choices: $R = a$, $R = b$, $R = (a+b)/2$, $R = \sqrt{ab}$, i.e. the two values of the semi-axes and the two means, the arithmetic and the geometric ones. We set $m_{max} = m_2 = 10$.

In Table 2 we report the convergence properties of two numerical tests, one for an ellipsoidal domain with a very low eccentricity ($a = 1.5$, $b = 1.2$), and the other one with a greater value of the eccentricity ($a = 3.0$, $b = 1.2$). The optimal values of σ_1 and σ_2 and the corresponding reduction factor have been found within the range of values belonging to a straight line, as described above. From

	ρ_0	σ_1^{opt}	σ_2^{opt}	# iter	ρ_0	σ_1^{opt}	σ_2^{opt}	# iter
$R = a$	0.12	4.57	-2.18	11	0.04	3.30	-1.47	9
$R = b$	0.15	5.14	-2.51	12	0.15	5.14	-2.51	13
$R = \frac{a+b}{2}$	0.13	4.83	-2.32	11	0.08	3.87	-1.78	10
$R = \sqrt{(ab)}$	0.14	4.84	-2.33	11	0.09	4.06	-1.89	11

Table 2: Number of iterations for the ellipsoidal domain. Left: $a = 1.5$, $b = 1.2$. Right: $a = 3.0$, $b = 1.2$. Test II.

these results, we observe that when the eccentricity is low, all the choices proposed to estimate R in the optimization procedure work well. For an increased

eccentricity, we observe instead some differences among the four choices, in particular $R = a$, i.e. approximating R with the length of the longest semi-axis, seems to produce better results.

5   The fluid-structure interaction problem

In the second part of the work, we focus on the fluid-structure interaction problem. The analysis and optimization procedure we are going to show will allow us to develop effective Robin-Robin algorithms for the solution of the FSI problem, when spherical-like interfaces separate fluid and structure. We are here interested in hemodynamics, in particular in the FSI problem arising between blood and vessel wall in an abdominal aortic aneurysm (AAA), i.e. a pathological enlargement of the abdominal aorta which in many cases assumes an almost spherical-like shape [31, 37].

In the following sections, we will provide a convergence analysis for a simplified FSI problem and then report the convergence properties of some numerical experiments, for a spherical domain and for a real AAA domain.

5.1   Problem setting

In view of the theoretical analysis, we consider a simplified problem arising from the interaction between the equations describing an incompressible, inviscid and linear fluid occupying the sphere $\Omega_f = \{\boldsymbol{x} \in \mathbb{R}^3 : x^2+y^2+z^2 < R^2\}$, and the wave equation (used as a simplified model for the linear elastic structure problem) occupying the spherical shell $\Omega_s = \{\boldsymbol{x} \in \mathbb{R}^3 : R^2 < x^2+y^2+z^2 < (R+H)^2\}$. The two subproblems interact at the common interface $\Sigma = \{\boldsymbol{x} \in \mathbb{R}^3 : x^2+y^2+z^2 = R^2\}$. The external surface is denoted by Σ_{out} and $\boldsymbol{n}$ is the outward unit normal.

The problem we are considering at discrete time $t^{n+1} = (n+1)\Delta t$ is the following:

$$\rho_f \delta_t \boldsymbol{u} + \nabla p = \boldsymbol{0} \qquad\qquad \text{in } \Omega_f, \qquad (15\text{a})$$

$$\nabla \cdot \boldsymbol{u} = 0 \qquad\qquad \text{in } \Omega_f, \qquad (15\text{b})$$

$$\boldsymbol{u} \cdot \boldsymbol{n} = \delta_t \boldsymbol{\eta} \cdot \boldsymbol{n} \qquad\qquad \text{on } \Sigma, \qquad (15\text{c})$$

$$-p = \lambda \nabla \boldsymbol{\eta} \boldsymbol{n} \cdot \boldsymbol{n} \qquad\qquad \text{on } \Sigma, \qquad (15\text{d})$$

$$\boldsymbol{\eta} \times \boldsymbol{n} = \boldsymbol{0} \qquad\qquad \text{on } \Sigma, \qquad (15\text{e})$$

$$\rho_s \delta_{tt} \boldsymbol{\eta} - \lambda \Delta \boldsymbol{\eta} = \boldsymbol{0} \qquad\qquad \text{in } \Omega_s, \qquad (15\text{f})$$

$$\gamma_{ST} \boldsymbol{\eta} + \lambda \nabla \boldsymbol{\eta} \boldsymbol{n} = P_{ext} \boldsymbol{n} \qquad\qquad \text{on } \Sigma_{out}, \qquad (15\text{g})$$

where $\boldsymbol{u}$ and p stand for fluid velocity and pressure, $\boldsymbol{\eta}$ represents the structure displacement, ρ_f and ρ_s are the fluid and structure densities, λ the coefficient related to the wave propagation that surrogates the elastic properties of the material, $\delta_t w = \frac{w - w^n}{\Delta t}$ and $\delta_{tt} w = \frac{\delta_t w - \delta_t w^n}{\Delta t}$, with Δt the time discretization step,

and where the current temporal index $n + 1$ is understood. Equations (15a)-(15b) represent the fluid problem, (15f)-(15g) the structure problem equipped with a Robin condition at the external surface to account for the effect of an elastic surrounding tissue with elasticity modulus γ_{ST}. P_{ext} is an external pressure. Conditions (15c) and (15d) represent the coupling conditions at the fluid-structure interface. Notice that owing to the inviscid nature of the fluid, the coupling at the interface occurs only in the normal direction. For this reason, we have to complete the boundary conditions for the structure problem along the tangential direction, for example by means of (15e).

Proceeding as above, we introduce two linear combinations of (15c) and (15d) by means of the interface operators S_f and S_s, obtaining the following generalized Robin interface conditions:

$$S_f u_r - p = S_f \delta_t \eta_r + \lambda \partial_r \eta_r,$$
$$S_s \delta_t \eta_r + \lambda \partial_r \eta_r = S_s u_r - p,$$

where $u_r = \boldsymbol{u} \cdot \boldsymbol{n}$, $\eta_r = \boldsymbol{\eta} \cdot \boldsymbol{n}$. Rearranging the previous conditions, we can write them equivalently as follows:

$$S_f \Delta t \delta_t u_r - p = \frac{S_f}{\Delta t} \eta_r + \lambda \partial_r \eta_r + F_1(u_r^n, \eta_r^n), \tag{16a}$$

$$\frac{S_s}{\Delta t} \eta_r + \lambda \partial_r \eta_r = S_s \Delta t \delta_t u_r - p + F_2(u_r^n, \eta_r^n), \tag{16b}$$

where F_1, F_2 contain terms at the previous time step n.

The FSI problem described by (15a)-(15g) can be equivalently rewritten by considering (16a) and (16b) as interface conditions. Thus, the Generalized Schwarz algorithm corresponding to problem given by (15a)-(15b)-(15e)-(15f)-(15g)-(16a)-(16b) reads as follows:
Set $\eta_r^{(0)} = \eta_r^n$. Then, at each iteration $k > 0$, until convergence

1. Solve the fluid problem:

$$\rho_f \delta_t \boldsymbol{u}^{(k)} + \nabla p^{(k)} = \boldsymbol{0} \qquad \text{in } \Omega_f, \tag{17a}$$
$$\nabla \cdot \boldsymbol{u}^{(k)} = 0 \qquad \text{in } \Omega_f,$$
$$S_f \Delta t \delta_t u_r^{(k)} - p^{(k)} = \frac{S_f}{\Delta t} \eta_r^{(k-1)} + \lambda \partial_r \eta_r^{(k-1)} + F_1(u_r^n, \eta_r^n) \qquad \text{on } \Sigma;$$

2. Then, solve the structure problem

$$\rho_s \delta_{tt} \boldsymbol{\eta}^{(k)} - \lambda \Delta \boldsymbol{\eta}^{(k)} = \boldsymbol{0} \qquad \text{in } \Omega_s,$$
$$\gamma_{ST} \boldsymbol{\eta}^{(k)} + \lambda \nabla \boldsymbol{\eta}^{(k)} \boldsymbol{n} = P_{ext} \boldsymbol{n} \qquad \text{on } \Sigma_{out},$$
$$\frac{S_s}{\Delta t} \eta_r^{(k)} + \lambda \partial_r \eta_r^{(k)} = S_s \Delta t \delta_t u_r^{(k)} - p^{(k)} + F_2(u_r^n, \eta_r^n) \qquad \text{on } \Sigma,$$
$$\boldsymbol{\eta}^{(k)} \times \boldsymbol{n} = \boldsymbol{0} \qquad \text{on } \Sigma.$$

12

5.2 Convergence analysis

In view of the convergence analysis of the previous algorithm, we first note that as usual we can refer to the homogeneous case, thus we set to zero the quantities at previous time steps. Moreover, by applying the divergence operator to the first of (17), we face with a laplacian problem for the pressure solely. Finally, starting again from (17a), we exploit that at the interface

$$(\rho_f \delta_t \boldsymbol{u} + \nabla p) \cdot \boldsymbol{n} \,|_\Sigma = 0,$$

leading to

$$\partial_r p|_\Sigma = -\rho_f \delta_t u_r|_\Sigma.$$

From these observations, the Generalized Schwarz algorithm (17)- (18) could be written as follows:

Set $\eta_r^{(0)} = \eta_r^n$. Then, at each iteration $k > 0$, until convergence

1. Solve the fluid problem:

$$\triangle p^{(k)} = 0 \qquad\qquad\qquad \text{in } \Omega_f,$$

$$- S_f \frac{\Delta t}{\rho_f} \partial_r p^{(k)} - p^{(k)} = \frac{S_f}{\Delta t} \eta_r^{(k-1)} + \lambda \partial_r \eta_r^{(k-1)} \qquad \text{on } \Sigma; \quad (19a)$$

2. Then, solve the structure problem

$$\frac{\rho_s}{\Delta t^2} \boldsymbol{\eta}^{(k)} - \lambda \Delta \boldsymbol{\eta}^{(k)} = \boldsymbol{0} \qquad\qquad \text{in } \Omega_s,$$

$$\gamma_{ST} \boldsymbol{\eta}^{(k)} + \lambda \nabla \boldsymbol{\eta}^{(k)} \boldsymbol{n} = P_{ext} \boldsymbol{n} \qquad\qquad \text{on } \Sigma_{out}, \qquad (20a)$$

$$\frac{S_s}{\Delta t} \eta_r^{(k)} + \lambda \partial_r \eta_r^{(k)} = -S_s \frac{\Delta t}{\rho_f} \partial_r p^{(k)} - p^{(k)} \qquad\qquad \text{on } \Sigma, \qquad (20b)$$

$$\boldsymbol{\eta}^{(k)} \times \boldsymbol{n} = \boldsymbol{0} \qquad\qquad \text{on } \Sigma.$$

We have he following result.

Proposition 2. *Set*

$$
\begin{aligned}
A(m) &= -\frac{\lambda \Delta t \left(2\beta \, R \, K'_{m+1/2}(\beta \, R) - K_{m+1/2}(\beta \, R) - \chi \left(2\beta \, R \, I'_{m+1/2}(\beta \, R) - I_{m+1/2}(\beta \, R) \right) \right)}{2R \left(K_{m+1/2}(\beta \, R) - \chi \, I_{m+1/2}(\beta \, R) \right)}, \\
B(m) &= -\frac{\rho_f \, R}{\Delta t \, m},
\end{aligned}
$$

$$(21)$$

where we have set

$$\beta = \sqrt{\frac{\rho_s}{\lambda \Delta t^2}}, \qquad\qquad (22)$$

and

$$\chi(m) = \frac{2\gamma_{ST}(R + H)K_{m+1/2}\left(\beta(R + H)\right) + 2\lambda\beta(R + H)K'_{m+1/2}(\beta(R + H)) - \lambda K_{m+1/2}\left(\beta(R + H)\right)}{2\gamma_{ST}(R + H)I_{m+1/2}\left(\beta(R + H)\right) + 2\lambda\beta(R + H)I'_{m+1/2}(\beta(R + H)) - \lambda I_{m+1/2}\left(\beta(R + H)\right)}. \qquad (23)$$

Then, the reduction factor of iterations (17)-(18) *is given by*

$$\rho(m) = \begin{cases} \left| \dfrac{\sigma_f(0) - A(0)}{\sigma_s(0) - A(0)} \right|, & \textit{if } m = 0, \\ \left| \dfrac{\sigma_f(m) - A(m)}{\sigma_s(m) - A(m)} \cdot \dfrac{\sigma_s(m) - B(m)}{\sigma_f(m) - B(m)} \right|, & \textit{if } m \neq 0, \end{cases} \qquad (24)$$

where σ_f and σ_s are the symbols of $\mathcal{S}_f$ and $\mathcal{S}_s$, respectively,

Proof. We start from the fluid problem. From (19) and applying the Fourier tranform (6) with (5), we obtain the following ordinary differential equations in the variable r:

$$r^2 \frac{\partial^2 \widehat{p}^{(k)}}{\partial r^2} + 2r \frac{\partial \widehat{p}^{(k)}}{\partial r} - m(m+1)\widehat{p}^{(k)} = 0.$$

The solution of the previous ODE is given by $\widehat{p}^{(k)}(r, m, l) = X_{f,1}^{(k)}(m, l)\, r^m + X_{f,2}^{(k)}(m, l)\, r^{-m-1}$, for suitable functions $X_{f,1}^{(k)}$ and $X_{f,2}^{(k)}$. Since, we assume that the pressure p is bounded for $r = 0$, we have

$$\widehat{p}^{(k)}(r, m, l) = X_f^{(k)}(m, l)\, r^m. \qquad (25)$$

Regarding the structure problem (18), by applying again the Fourier tranform (6) and (5), we face with an equation for η_r equal to (11) with $\frac{\rho_s}{\lambda \Delta t^2}$ instead of $\frac{\gamma}{\mu}$. Thus, the solution is given by $\widehat{\eta}_r^{(k)}(r, m, l) = X_{s,1}^{(k)}(m, l)\frac{I_{m+1/2}(\beta r)}{\sqrt{r}} + X_{s,2}^{(k)}(m, l)\frac{K_{m+1/2}(\beta r)}{\sqrt{r}}$ for suitable functions $X_{s,1}^{(k)}$ and $X_{s,2}^{(k)}$ and with β given by (22). Now, we impose condition (20a), leading to

$$\gamma_{ST} \left(X_{s,1}^{(k)} \frac{I_{m+1/2}(\beta r)}{\sqrt{r}} + X_{s,2}^{(k)} \frac{K_{m+1/2}(\beta r)}{\sqrt{r}} \right)$$
$$+\lambda \left(X_{s,1}^{(k)} \beta \frac{I'_{m+1/2}(\beta r)}{\sqrt{r}} - X_{s,1}^{(k)} \frac{I_{m+1/2}(\beta r)}{2\sqrt{r^3}} + X_{s,2}^{(k)} \beta \frac{K'_{m+1/2}(\beta r)}{\sqrt{r}} - X_{s,2}^{(k)} \frac{K_{m+1/2}(\beta r)}{2\sqrt{r^3}} \right)\Bigg|_{r=R+H} = 0,$$

and thus to $X_{s,1}^{(k)} = -\chi\, X_{s,2}^{(k)}$, where χ is given by (23). Therefore, the structure solution is

$$\widehat{\eta}_r^{(k)}(r, m, l) = X_s^{(k)}(m, l)\frac{1}{\sqrt{r}} \left[K_{m+1/2}(\beta r) - \chi(m) I_{m+1/2}(\beta r) \right]. \qquad (26)$$

By inserting the solutions (25) and (26) in the interface conditions (19a)-(20b), the thesis follows. $\qquad \square$

6 Numerical results for the fluid-structure interaction problem

6.1 Optimization procedure

In view of the numerical results, we need suitable values for the interface symbols S_f and S_s in the iterations (17)-(18). We proceed as done in Sect. 3, i.e. we

look for constant values along the straight line defined by (14), i.e. of the form

$$\begin{cases} \sigma_f = p, \\ \sigma_s = 2\overline{M} - p, \end{cases}$$

where p belongs to a suitable range $[p_-, p_+]$ and A and B are given by (21).

For the choice of the frequencies to be used in the optimization procedure, we consider all the frequencies $m \in [0, N-1]$, with $N = \sqrt{n}$ and n the number of interface nodes (see strategy 1 in Sect. 3) .

6.2 Problem setting

We present in what follows the fluid-structure interaction problem we are going to consider to validate the theoretical findings of the previous section. In particular, we are interested in hemodynamics where the large *added mass effect* due to the similarity of the densities makes the convergence of partitioned algorithms very challenging [6, 29].

We consider the coupling between the Navier-Stokes equations for an incompressible fluid solved in the *Arbitrary Lagrangian-Eulerian* formulation [10] and the linear infinitesimal elasticity. The main purpose here is to verify that the optimal interface parameters found for the simplified FSI problem analyzed in the previous section are effective also for the "complete" FSI problem. We have for each t:

$$\begin{aligned}
& \rho_f \partial_t^A \boldsymbol{u} + \rho_f ((\boldsymbol{u} - \boldsymbol{\omega}) \cdot \nabla) \boldsymbol{u} - \nabla \cdot \boldsymbol{T}_f(\boldsymbol{u}, p) = \boldsymbol{0} && \text{in } \Omega_f, \\
& \nabla \cdot \boldsymbol{u} = 0 && \text{in } \Omega_f, \\
& \rho_s \partial_{tt} \widehat{\boldsymbol{\eta}} - \nabla \cdot \widehat{\boldsymbol{T}}_s(\widehat{\boldsymbol{\eta}}) = \boldsymbol{0} && \text{in } \widehat{\Omega}_s, \quad \text{(27a)} \\
& \boldsymbol{u} = \delta_t \boldsymbol{\eta} && \text{on } \Sigma, \\
& \boldsymbol{T}_f \boldsymbol{n} - \boldsymbol{T}_s \boldsymbol{n} = \boldsymbol{0} && \text{on } \Sigma,
\end{aligned}$$

where $\boldsymbol{T}_f(\boldsymbol{u}, p) = -p\boldsymbol{I} + \mu(\nabla \boldsymbol{u} + (\nabla \boldsymbol{u})^T)$ is the Cauchy stress tensor for the fluid, with μ the dynamic viscosity. Moreover, ∂_t^A represents the ALE derivative, i.e. the time derivative in the Arbitrary Lagrangian-Eulerian framework, and $\boldsymbol{\omega}$ is the velocity of the fluid domain obtained by solving an harmonic extension of the interface velocity with homogeneous Dirichlet boundary conditions on $\Omega_f \setminus \Sigma$. Notice that, accordingly, Ω_f changes in time. Instead, the structure problem (27a) is solved in a Lagrangian framework and for this reason we have indicated with $\widehat{}$ the corresponding quantities. Moreover, $\boldsymbol{T}_s$ is the structure Cauchy stress tensor given by

$$\boldsymbol{T}_s(\boldsymbol{\eta}) = \lambda_1(\nabla \boldsymbol{\eta} + (\nabla \boldsymbol{\eta})^T) + \lambda_2(\nabla \cdot \boldsymbol{\eta})\boldsymbol{I},$$

where λ_1 and λ_2 are the Lamé constants, that can be defined in terms of the Young modulus E and the Poisson ratio ν as follows

$$\lambda_1 = \frac{E}{2(1+\nu)}, \quad \lambda_2 = \frac{\nu E}{(1+\nu)(1-2\nu)}.$$

15

We assume that the value of λ in the simplified structure problem (15f) is approximated by $\lambda = G\lambda_1$, where $G = \frac{\pi}{12}$ is the Timoshencko correction factor [16].

We use the following values for parameters: $\mu = 0.035\,g/(cm\,s)$, $\rho_f = 1.0\,g/cm^3$, $\rho_s = 1.1\,g/cm^3$, $\nu = 0.49$, $E = 3 \cdot 10^6\,dyne/cm^2$, $\Delta t = 10^{-3}s$. Accordingly, we have $\lambda = 8.3 \cdot 10^5\,g/(cm\,s^2)$.

We consider a backward Euler time discretization with a semi-implicit treatment of the convective term for the fluid and the BDF1 scheme for the structure. Moreover, we consider a semi-implicit treatment also for the geometric coupling, i.e. the fluid domain is found by extrapolation of previous time steps [4, 11, 28]. We use the pair of stable finite elements $P_{1,bubble} - P_1$ for the fluid subproblem and P_1 for the strucure subproblem. The convergence of the Robin-Robin algorithm has been monitored by evaluating at each iteration the following quantity [3]

$$\int_\Sigma \sigma_f \left| \boldsymbol{u}^{(k)} - \delta_t \boldsymbol{\eta}^{(k)} \right| + \left| \boldsymbol{T}_f(\boldsymbol{u}^{(k)}, p^{(k)}) - \boldsymbol{T}_s(\boldsymbol{\eta}^{(k)}) \right| < \varepsilon,$$

where the value of the tolerance parameter ε has been set equal to 10^{-7}.

The numerical simulations have been performed with the Finite Elements library *LIFEV* [1].

6.3 The case of spherical domain

We start considering an FSI test in a 3D sphere cut at two opposite sides where the inlet and outlet planar sections Γ_{in} and Γ_{out} are located, see the corresponding fluid mesh in Figure 3. We have $R = 0.5\,cm$ and $H = 0.1\,cm$, and the meshes
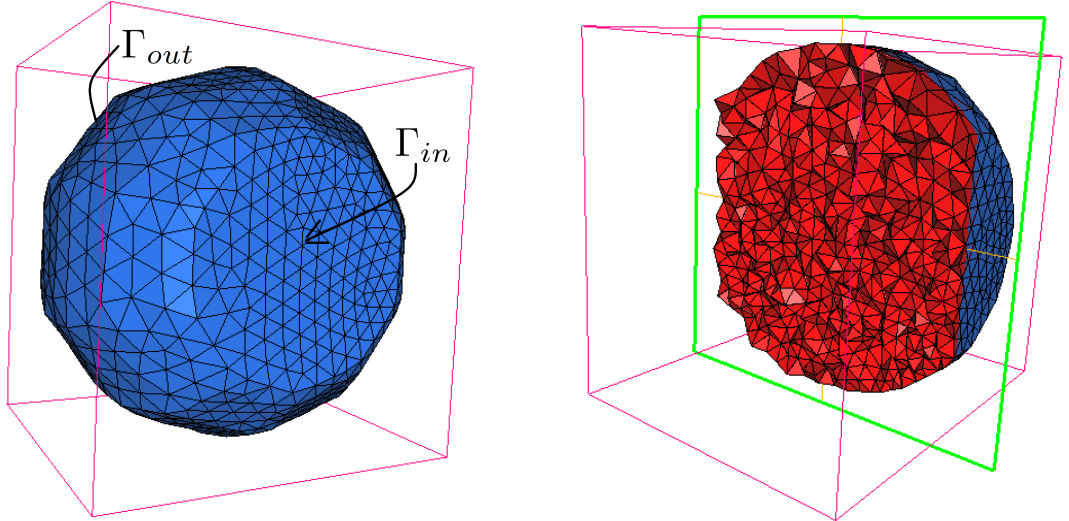

Figure 3: Computational fluid mesh for the FSI test in the sphere.

are such that the number of tetrahedra are about 33k for the fluid and 5k for the structure. Moreover, we have $N = 38$.

On the portion of Γ_{in} corresponding to the fluid domain, we prescribed the impulsive Neumann condition $\boldsymbol{T}_f(\boldsymbol{u}, p)\boldsymbol{n} = -P_{in}\boldsymbol{n}$, where

$$P_{in} = \begin{cases} 10 \, dyne/cm^2 & \text{for } t < 0.008s, \\ 0 & \text{for } 0.008s \leq t \leq T, \end{cases}$$

where $T = 0.020$ s. At the fluid outlet, we prescribed an absorbing boundary condition, see [28, 30]. For the structure, on both the inlet and outlet surfaces we prescribe $\boldsymbol{\eta} = \boldsymbol{0}$, i.e. we keep them fixed. Instead, at the external surface Γ_{ext}, we prescribe the Robin condition

$$\gamma_{ST}\widehat{\boldsymbol{d}} + \widehat{\boldsymbol{T}}_s(\widehat{\boldsymbol{d}})\widehat{\boldsymbol{n}} = \boldsymbol{0},$$

with $\gamma_{ST} = 1.5 \cdot 10^6 \, dyne/cm^3$, to account for the effect of the surrounding tissue [27].

In Figure 4 we report the pressure field at four different instants. We observe, as expected, the travelling pressure wave which is absorbed at the outlet.
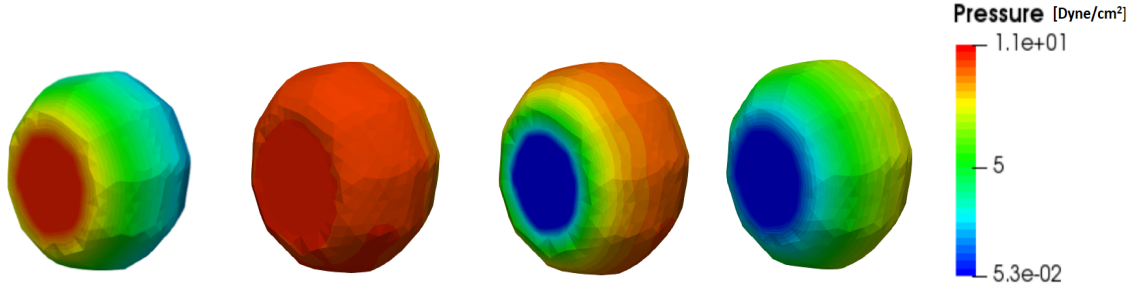

Figure 4: Pressure field at four different instants. From the left to the right: $t = 0.002\,s$, $t = 0.006\,s$, $t = 0.008\,s$, $t = 0.010\,s$. Γ_{in} on the left.

The optimization procedure leads to the estimation of the following optimal values, $\sigma_f = 1886.0$ and $\sigma_s = -17.3$. In Table 3 we report the convergence performance of the optimized Robin-Robin (RR) scheme and of the Dirichlet-Neumann (DN) scheme with an Aitken procedure. In particular, we consider variations of the Reynolds number (I and II rows), of Δt (I and III rows), and of the mesh (I and IV rows). The number of iterations is the average among the different time instants.

From these results we can observe a significant improvement of the convergence properties when optimal values of the interface parameters derived by our analysis are used in a RR scheme. In particular, this scheme works well in comparison to the DN scheme also for increased values of the Reynolds number and decreased values of Δt.

Notice also that the convergence properties of both RR and DN schemes deteriorate for decreasing values of Δt. This was expected for the DN scheme,

	Method	σ_f/σ_s	# Iter
P_{in}, Δt	Optimized RR	$1886.0/-17.3$	5.8
$N = 38$	DN+Aitken	$+\infty/0$	11.6
$100P_{in}$, Δt	Optimized RR	$1886.0/-17.3$	7.8
$N = 38$	DN+Aitken	$+\infty/0$	14.1
P_{in}, $\Delta t/10$	Optimized RR	$1002.2/-186.6$	15.2
$N = 38$	DN+Aitken	$+\infty/0$	28.6
P_{in}, Δt	Optimized RR	$1887.4/-16.8$	5.9
$N = 44$	DN+Aitken	$+\infty/0$	11.9

Table 3: Convergence performance for different valus of P_{in} and Δt and different meshes. FSI test in the sphere.

indeed from (24) we have that $\lim_{\Delta t \to 0} \rho = 1$ when $\sigma_f = +\infty$ and $\sigma_s = 0$. Instead, for the RR scheme we could in principle choose σ_f and σ_s such that $\lim_{\Delta t \to 0} \rho < 1$. This is confirmed by the values reported in Table 4, showing an a priori estimate of the optimal value ρ_{opt} of ρ and of the corresponding values of σ_f and σ_s (these being slightly different from those in Tab. 3 since the latter where estimated heuristically). These results show that the convergence

Δt	σ_f	σ_s	ρ_{opt}
10^{-3}	1947.2	-77.6	0.033
10^{-4}	1049.4	-233.0	0.083
10^{-5}	986.7	-1365.9	0.006
10^{-6}	955.8	-13512.2	0.0001

Table 4: Values of the estimated optimal value ρ_{opt} as a function of Δt. FSI test in the sphere.

properties of the RR scheme with optimal interface parameters deteriorate in accordance with the numerical results when $\Delta t \geq 10^{-4}$, however they improve for smaller values of Δt.

Finally, we notice that, as expected by the theory [35], for both RR and DN methods the number of iterations is quite independent of the mesh size.

6.4 The case of an abdominal aortic aneurysm

In the second test, we aim at applying our optimization procedure for the Robin-Robin scheme to a case of a real aortic aneurysm, namely one that develops at the abdominal level. These aneurysms could be in principle characterized by a baloon-like shape or could be fusiform, i.e. extended along the axial direction. In the first case, the almost spherical shape of the domain suggests the use of the analysis developed above to improve an FSI simulation.

To this aim, we consider the geometry of a real patient, see Figure 5. We use the same physical parameters and boundary conditions of the previous test
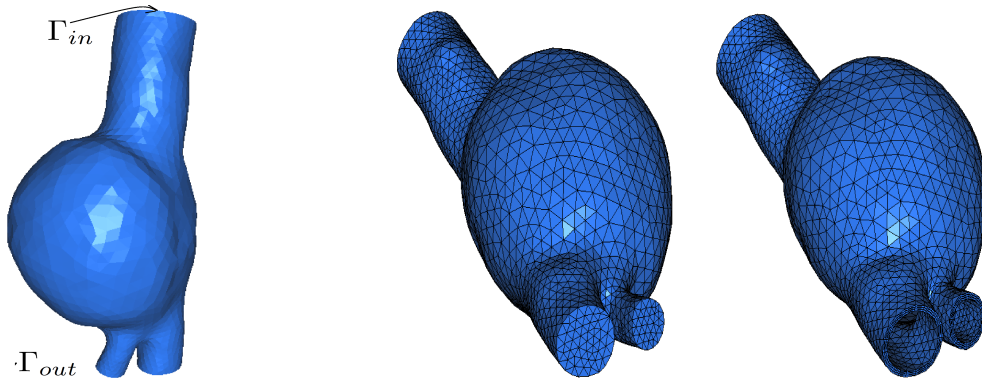
Figure 5: Domain of the aortic aneurysm (left) and fluid and structure meshes (right).

case. The fluid and structure meshes are conforming at the interface and the number of tetrahedra is about 54k for the fluid and about 34k for the structure. The values of the representative radius and thickness used in the optimization procedure are $R = 2.3\,cm$ and $H = 0.1\,cm$. Moreover, we have $N = 23$.

In Figure 6 we report the pressure field at four different instants. Again, as expected, the pressure wave travels along the domain and is absorbed at the outlet.
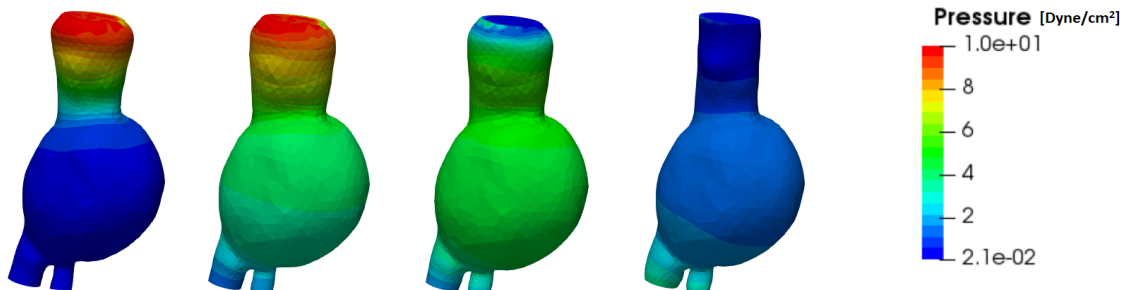

Figure 6: Pressure field at four different instants. From the left to the right: $t = 0.002\,s$, $t = 0.006\,s$, $t = 0.008\,s$, $t = 0.010\,s$.

From the optimization procedure, we found that the optimal values are $\sigma_f = 1511.0$ and $\sigma_s = -143.4$. The number of iterations to reach convergence (average number among the different time instants) is in this case 12.0 against 15.6 needed by the DN-Aitken scheme. The improvement is more restrained in this case with respect to the previous test, probably because the geometry is not a perfect sphere as in the previous case. However, we have a speed-up of about 23%. This means that, since the number of iterations is quite independent of the mesh size, for more refined meshes needed for clinical applications, when the overall computational effort could be even of days, the speed-up of the RR

scheme is in absolute very significant.

Acknowledgement

References

[1] www.lifev.org.

[2] S. Ali Hassan, C. Japhet, and M. Kern M. Vohralk. A posteriori stopping criteria for optimized schwarz domain decomposition algorithms in mixed formulations. *Computational Methods in Applied Mathematics*, 18(3):495 – 520, 2018.

[3] S. Badia, F. Nobile, and C. Vergara. Fluid-structure partitioned procedures based on Robin transmission conditions. *J. Comput. Physics*, 227:7027–7051, 2008.

[4] S. Badia, A. Quaini, and A. Quarteroni. Splitting methods based on algebraic factorization for fluid-structure interaction. *SIAM J. Sci. Comp.*, 30(4):1778–1805, 2008.

[5] E. Blayo, D. Cherel, and A. Rousseau. Towards optimized schwarz methods for the navierstokes equations. *Journal of Scientific Computing*, 66(1):275 – 295, 2016.

[6] P. Causin, J.F. Gerbeau, and F. Nobile. Added-mass effect in the design of partitioned algorithms for fluid-structure problems. *Comput. Methods Appl. Mech. Engrg.*, 194(42-44):4506–4527, 2005.

[7] S. Deparis. *Numerical analysis of axisymmetric flows and methods for fluid-structure interaction arising in blood flow simulation.* PhD thesis, École Polytechnique Fédérale de Lausanne, 2004.

[8] M. Discacciati and L. Gerardo-Giorda. Optimized schwarz methods for the stokesdarcy coupling. *IMA Journal of Numerical Analysis*, 38(4):1959 – 1983, 2018.

[9] V. Dolean, M.J. Gander, and L. Gerardo Giorda. Optimized Schwarz Methods for Maxwell's equations. *SIAM J. Sci. Comp.*, 31(3):2193–2213, 2009.

[10] J. Donea. An arbitrary Lagrangian-Eulerian finite element method for transient dynamic fluid-structure interaction. *Comput. Methods Appl. Mech. Engrg.*, 33:689–723, 1982.

[11] M.A. Fernández, J.F. Gerbeau, and C. Grandmont. A projection semi-implicit scheme for the coupling of an elastic structure with an incompressible fluid. *Int. J. Num. Methods Engrg.*, 69(4):794–821, 2007.

[12] G.B. Folland. *Introduction to partial differential equations.* Princeton University press, 1995.

[13] M.J. Gander. Optimized Schwarz Methods. *SIAM J. Numer. Anal.*, 44(2):699–731, 2006.

[14] M.J. Gander and Y. Xu. Optimized Schwarz Methods for circular domain decompositions with overlap. *SIAM J. Numer. Anal.*, 52(4):19812004, 2014.

[15] M.J. Gander and Y. Xu. Optimized schwarz methods with nonoverlapping circular domain decomposition. *Math. Comp.*, 86(304):637 – 660, 2017.

[16] L. Gerardo Giorda, F. Nobile, and C. Vergara. Analysis and optimization of Robin-Robin partitioned procedures in fluid-structure interaction problems. *SIAM J. Numer. Anal.*, 48(6):2091–2116, 2010.

[17] G. Gigante, M. Pozzoli, and C. Vergara. Optimized Schwarz Methods for the diffusion-reaction problem with cylindrical interfaces. *SIAM J. Numer. Anal.*, 51(6):3402–3420, 2013.

[18] G. Gigante and C. Vergara. Analysis and optimization of the generalized Schwarz method for elliptic problems with application to fluid-structure interaction. *Numer. Math.*, 131(2):369–404, 2015.

[19] G. Gigante and C. Vergara. Optimized Schwarz method for the fluid-structure interaction with cylindrical interfaces. In T. Dickopf, M.J. Gander, L. Halpern, R. Krause, and L.F. Pavarino, editors, *Proceedings of the XXII International Conference on Domain Decomposition Methods*, pages 521–529. Springer, 2016.

[20] G. Gigante and C. Vergara. Optimized schwarz methods for the coupling of cylindrical geometries along the axial direction. *Mathematical Modelling and Numerical Analysis*, 52:1597–1615, 2018.

[21] C. Japhet. Optimized Krylov-Ventcell method. Application to convection-diffusion problems. In P.E. Bjorstad, M.S. Espedal, and D.E. Keyes, editors, *Proceedings of the Ninth International Conference on Domain Decomposition Methods*, pages 382–389, 1998.

[22] N. Lebedev. *Special Functions and Their Applications.* Courier Dover Publications, 1972.

[23] P.L. Lions. On the Schwarz alternating method III. In T. Chan, R. Glowinki, J. Periaux, and O.B. Widlund, editors, *Proceedings of the Third International Symposium on Domain Decomposition Methods for PDE's*, pages 202–223. Siam, Philadelphia, 1990.

[24] S.H. Lui. A lions non-overlapping domain decomposition method for domains with an arbitrary interface. *IMA Journal of Numerical Analysis*, 29(2):332 – 349, 2009.

[25] F. Magoules, A.K. Cheik Ahamed, and R. Putanowicz. Optimized schwarz method without overlap for the gravitational potential equation on cluster of graphics processing unit. *International Journal of Computer Mathematics*, 93(6):332 – 349, 2016.

[26] F. Magoules, D.B. Szyld, and C. Venet. Asynchronous optimized schwarz methods with and without overlap. *Numer. Math.*, 137:199 – 227, 2017.

[27] P. Moireau, N. Xiao, M. Astorino, C. A. Figueroa, D. Chapelle, C. A. Taylor, and J.-F. Gerbeau. External tissue support and fluidstructure simulation in blood flows. *Biomechanics and Modeling in Mechanobiology*, 11(1-2):1–18, 2012.

[28] F. Nobile, M. Pozzoli, and C. Vergara. Time accurate partitioned algorithms for the solution of fluid-structure interaction problems in haemodynamics. *Computer & Fluids*, 86:470–482, 2013.

[29] F. Nobile, M. Pozzoli, and C. Vergara. Inexact accurate partitioned algorithms for fluid-structure interaction problems with finite elasticity in haemodynamics. *Journal of Computational Physics*, 273:598–617, 2014.

[30] F. Nobile and C. Vergara. An effective fluid-structure interaction formulation for vascular dynamics by generalized Robin conditions. *SIAM J. Sci. Comp.*, 30(2):731–763, 2008.

[31] M. Piccinelli, C. Vergara, L. Antiga, L. Forzenigo, P. Biondetti, and M. Domanin. Impact of hemodynamics on lumen boundary displacements in abdominal aortic aneurysms by means of dynamic computed tomography and computational fluid dynamics. *Biomech Model Mechanobiol*, 2013.

[32] A. Qaddouria, L. Laayounib, S. Loiselc, J Cotea, and M.J. Gander. Optimized Schwarz methods with an overset grid for the shallow-water equations: preliminary results. *Appl. Num. Math*, 58:459–471, 2008.

[33] A. Quarteroni, L. Dede', A. Manzoni, and C. Vergara. *Mathematical Modelling of the Human Cardiovascular System - Data, Numerical Approximation, Clinical Applications*. Cambridge University Press, 2019.

[34] A. Quarteroni, R. Sacco, and F. Saleri. *Numerical mathematics.* Springer Berlin, 2000.

[35] A. Quarteroni and A. Valli. *Domain Decomposition Methods for Partial Differential Equations.* Oxford Science Publications, 1999.

[36] B. Stupfel. Improved transmission conditions for a one-dimensional domain decomposition method applied to the solution of the Helmhotz equation. *J. Comput. Physics*, 229:851–874, 2010.

[37] C.A. Taylor, T.J.R. Hughes, and C.K. Zarins. Finite element analysis of pulsatile flow in the abdominal aorta under resting and exercise conditions. *American Society of Mechanical Engineers, Bioengineering Division*, 33:81–82, 1996.

[38] Y. Yu, H. Baek, and G.E. Karniadakis. Generalized fictitious methods for fluid-structure interactions: Analysis and simulations. *J. Comput. Physics*, 245:317–346, 2013.

MOX Technical Reports, last issues

Dipartimento di Matematica
Politecnico di Milano, Via Bonardi 9 - 20133 Milano (Italy)

21/2019   Martino, A.; Guatteri, G.; Paganoni, A.M.
Hidden Markov Models for multivariate functional data

20/2019   Martino, A.; Guatteri, G.; Paganoni, A.M.
Hidden Markov Models for multivariate functional data

18/2019   Delpopolo Carciopolo, L.; Cusini, M.; Formaggia, L.; Hajibeygi, H.
Algebraic dynamic multilevel method with local time-stepping (ADM-LTS) for sequentially coupled porous media flow simulation

19/2019   Torti, A.; Pini, A.; Vantini, S.
Modelling time-varying mobility flows using function-on-function regression: analysis of a bike sharing system in the city of Milan.

17/2019   Antonietti,P.F.; De Ponti, J.; Formaggia, L.; Scotti, A.
Preconditioning techniques for the numerical solution of flow in fractured porous media

14/2019   Antonietti, P.F.; Facciolà, C; Verani, M.
Mixed-primal Discontinuous Galerkin approximation of flows in fractured porous media on polygonal and polyhedral grids

15/2019   Brandes Costa Barbosa, Y. A.; Perotto, S.
Hierarchically reduced models for the Stokes problem in patient-specific artery segments

16/2019   Antonietti, P.F.; Houston, P.; Pennesi, G.; Suli, E.
An agglomeration-based massively parallel non-overlapping additive Schwarz preconditioner for high-order discontinuous Galerkin methods on polytopic grids

13/2019   Manzoni, A; Quarteroni, A.; Salsa, S.
A saddle point approach to an optimal boundary control problem for steady Navier-Stokes equations

09/2019   Antonietti, P.F.; Facciola', C.; Verani, M.
Unified analysis of Discontinuous Galerkin approximations of flows in fractured porous media on polygonal and polyhedral grids